Available online at www.sciencedirect.com
ScienceDirect
Procedia Engineering 2 (2010) 2141–2150
Procedia Engineering
www.elsevier.com/locate/procedia

Fatigue 2010

Influence of strain rate on P92 microstructural stability during fatigue tests at high temperature

P.F. Giroux[a,b,*], F. Dalle[a], M. Sauzay[a], C. Caës[a], B. Fournier[a], T. Morgeneyer[b], A.F. Gourgues-Lorenzon[b]

[a]*Commissariat à l'Énergie Atomique, DEN/DANS/DMN/SRMA, 91191 Gif-sur-Yvette Cedex, France*
[b]*Centre des Matériaux / MINES ParisTech, CNRS UMR 7633, B.P. 87, 91003 Évry Cedex, France*

Received 7 March 2010; revised 9 March 2010; accepted 15 March 2010

Abstract

9-12%Cr creep-resistant ferritic-martensitic steels are candidates for structural components of Generation IV nuclear power plants. However, they are sensitive to softening during fatigue and creep-fatigue loading. To better understand softening mechanisms in ASTM Grade 92, fatigue tests were carried out at 823 K at various strain amplitudes. Two different values of the strain rate ($2\ 10^{-3}\ s^{-1}$ and $10^{-5}\ s^{-1}$) were used for one strain amplitude. The softening behavior is mainly due to microstructural evolution. Examination of fractured specimens (hardness tests, TEM) shows an influence of strain rate on both increase in subgrain size and decrease in free dislocation density during cycling. Study of the evolution of isotropic, kinematic and viscous contributions to stress during fatigue tests shows a decrease in the kinematic contribution during cycling. A simplified mean field polycrystalline model based on subgrain growth is proposed in order to account for this strain rate effect. Potential impact on further creep resistance behavior is discussed.

Keywords: Grade 92 steel; fatigue tests; softening behavior; microstrural evolution; TEM; polycrystalline model

1. Introduction

Several grades of 9-12%Cr tempered martensitic steels are candidate materials for structural components for Generation IV nuclear power plants. They possess high strength and high thermal conductivity, low thermal expansion compared to austenitic steels, good corrosion resistance and interesting mechanical properties after irradiation [1-2]. However, they are sensitive to softening during high temperature mechanical loading such as low cycle fatigue, creep, and creep-fatigue [3-5]. Transmission electron microscopy (TEM) and electron backscatter diffraction (EBSD) performed with field-emission gun scanning electron microscope (FEG-SEM) observations showed that this phenomenon is mainly due to an increase in size of the microstructure and a decrease in free dislocation density during high-temperature deformation [6-8].

The strain rate seems to influence the microstructural stability of Grade 92 (9% Cr) steel at least during tensile

* Corresponding author. Tel.: +33 01 69 08 78 93; fax: +33 01 69 08 71 67.
E-mail address: pierre-francois.giroux@cea.fr

1877-7058 © 2010 Published by Elsevier Ltd.
doi:10.1016/j.proeng.2010.03.230

tests [9]. The purpose of the present work is to focus on the influence of strain rate on microstructural stability of Grade 92 steel during pure fatigue (PF) tests at 823K.

Besides TEM observations of specimens after fatigue tests, a possible way to identify the main physical mechanisms inducing softening is partitioning of the macroscopic cyclic stress between "isotropic", "kinematic" and "viscous" contributions [10]. Finally, a simplified mean field polycrystalline model based on Kröner's approach [11] is proposed. Using physical parameters mainly determined by microstructural observations, the model describes the evolution of the dislocation structure. The results are discussed and some prospects are proposed in order to improve the model.

2. Low cycle fatigue results

2.1. Pure Fatigue tests

Pure fatigue tests were conducted on Grade 92 steel specimens taken from a pipe of 219 mm in outer diameter and 20 mm in thickness. Its chemical composition is given in Table 1. The as-received material had been austenized at 1333 K for 30 min, quenched and tempered at 1043 K for 60 min.

Table 1. Chemical composition of the studied Grade 92 steel (in wt%)

Elements	C	N	Cr	Mo	W	Mn	V	Si	Ni	Al	Nb	P	S	B
Wt. (%)	0.12	0.046	8.68	0.37	1.59	0.54	0.19	0.23	0.26	0.02	0.06	0.014	0.004	0.002

All PF tests were performed in air at 823 K using a MAYES ESM100 servo-mechanical machine with resistance furnace heating. They were conducted on smooth cylindrical specimens with 16 mm in gauge length, 8 mm in gauge diameter and a shoulder radius of 16 mm, machined from mid-thickness of the pipe along its longitudinal axis. The temperature along the gauge part of the specimen was controlled within ±2 K. PF tests were performed with a control of axial strain, measured by a capacitive extensometer (10 mm in gauge length) directly attached on the gauge part of the specimen. The accuracy of elongation measurements is better than 0.5 µm, allowing PF tests with a total strain range as small as 0.1 % to be conducted. Ten PF tests were carried out at $2\ 10^{-3}\ s^{-1}$ for various fatigue strain ranges (Table 2). Additionally, one PF test was performed at $10^{-5}\ s^{-1}$ for a strain range of 0.70 %.

Fig. 1 presents the relationship between plastic strain range and fatigue lifetime N_{50} for Grade 91 and Grade 92 steels in similar conditions (except for test 11 at $10^{-5}\ s^{-1}$). For a given imposed strain rate, no significant difference between Grade 91 and Grade 92 steels is observed: the Manson-Coffin parameters of each adjusted curves do not differ significantly with respect to experimental scatter . Moreover, although only one PF test was carried out at $10^{-5}\ s^{-1}$ on Grade 92 steel, it seems that the strain rate has no significant influence on fatigue lifetime.

2.2. Cyclic softening curves

The study of the 10 PF tests carried out at $2\ 10^{-3}\ s^{-1}$ for various strain ranges from 1.00 % to 0.40 % of total strain showed that softening is more pronounced for higher strain range values: the higher the strain range, the more pronounced the softening effect.

To study the influence of strain rate on P92 cyclic softening, this work will now focus on tests 3 and 11 whose conditions are the same except for the strain rate. Fig. 2 presents four hysteresis loops recorded at the 1^{st}, 10^{th}, 100^{th} and $1{,}000^{th}$ cycle for each test.

Table 2. PF tests results on Grade 92 steel. ΔE is the macroscopic strain range and ΔE_p is its plastic part. N_f and N_{50} are the number of fatigue cycles to fracture and leading to a 50 % decrease in maximum stress, respectively.

Tests	Strain rate (s^{-1})	ΔE (%)	ΔE_p (%)	N_{50}	N_f
1	$2\ 10^{-3}$	1.00	0.610	1,872	2,291
2	$2\ 10^{-3}$	1.00	0.618	2,225	2,392
3	$2\ 10^{-3}$	0.70	0.335	4,450	4,552
4	$2\ 10^{-3}$	0.70	0.334	5,193	6,689
5	$2\ 10^{-3}$	0.60	0.245	7,613	8,545
6	$2\ 10^{-3}$	0.60	0.242	8,482	9,786
7	$2\ 10^{-3}$	0.50	0.155	12,957	13,450
8	$2\ 10^{-3}$	0.50	0.158	15,374	15,961
9	$2\ 10^{-3}$	0.40	0.083	144,766	157,017
10	$2\ 10^{-3}$	0.40	0.089	169,793	170,829
11	10^{-5}	0.70	0.376	3,793	3,960

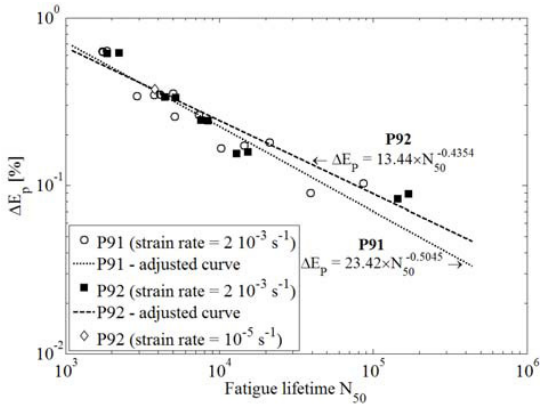

Fig. 1. Manson-Coffin curves for Grade 91 [12] and Grade 92 steels at 823 K.

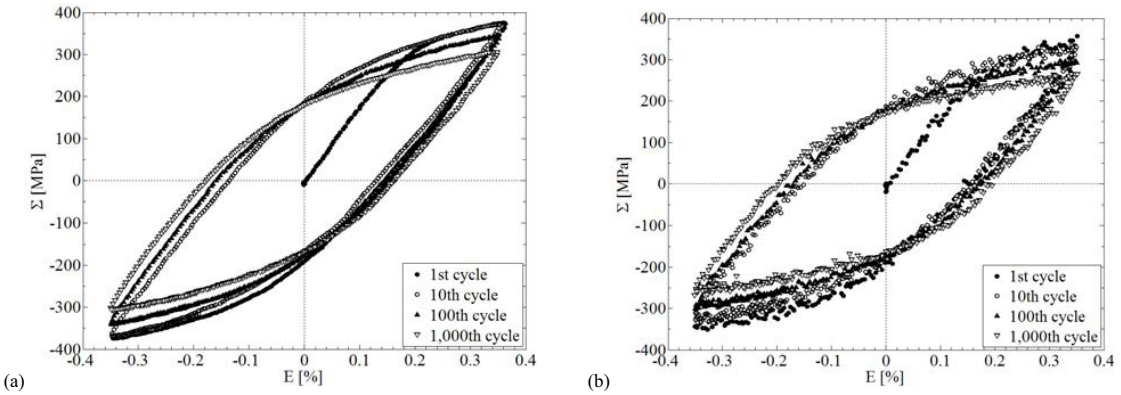

Fig. 2. Hysteresis loops recorded at 1st, 10th, 100th and 1,000th cycles of PF for (a) test 3 and (b) test 11.

Although hysteresis loops of test 11 are affected by some noise (Fig. 2(b)), cyclic softening is significant for both strain rates (Figs. 2 and 3) and the stress range decreases faster for the lower strain rate (Fig. 3(b)). This result means that the studied material is more sensitive to softening for lower strain rates.

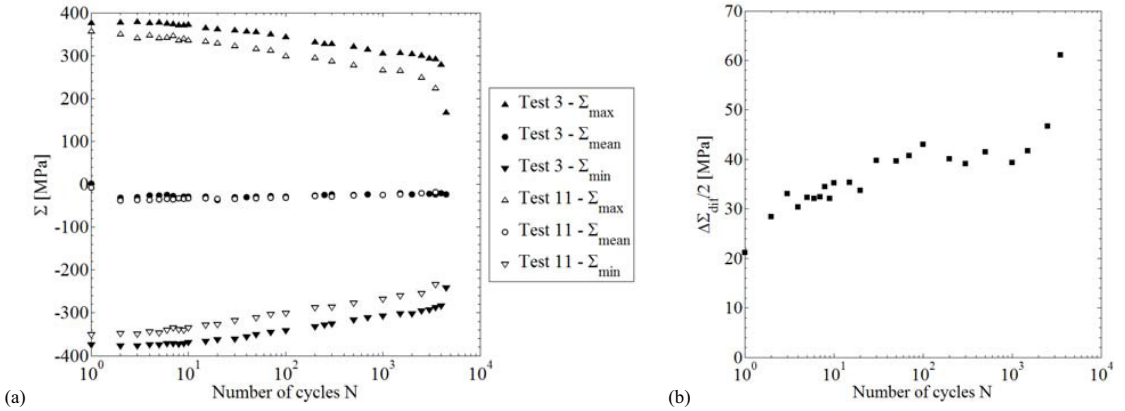

Fig. 3. (a) Evolution of maximum, minimum and mean stresses for test 3 and test 11 and (b) evolution of the difference between stress range of test 3 and stress range of test 11: $\Delta\Sigma_{dif}(N) = \Delta\Sigma^{test\ 3}(N) - \Delta\Sigma^{test\ 11}(N)$ with $\Delta\Sigma(N) = \Sigma_{max}(N) - \Sigma_{min}(N)$ for each test.

2.3. Analysis of softening

To improve the understanding of strain rate sensitivity during PF tests, evolution of the isotropic (R), the kinematic (X) and the viscous parts (Σ_v) of the macroscopic stress have been studied. This partition is used to investigate the mechanisms responsible for the mechanical behavior of crystalline materials under cyclic loading [13]. On the one hand, the effective stress, corresponding to the sum of the isotropic and viscous parts, corresponds to short-range interactions and is assimilated to the stress required to move a dislocation. On the other hand, the kinematic stress corresponds to long-range interactions (subgrain boundary effects, strain incompatibilities…) [12]. A method developed by Fournier et al. for highly viscous materials [12] is used to extract and study the evolution of the three components during test 3 (Fig. 4).

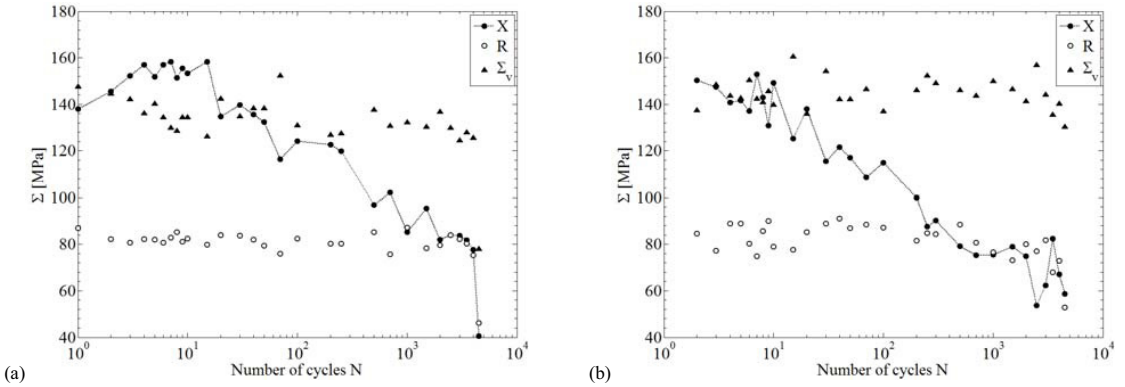

Fig. 4. Evolution of the kinematic (X), isotropic (R) and viscous (Σ_v) contributions to total stress for test 3 (a) in compression and (b) in tension

Both in compression and in tension, R and Σ_v are constant during the test: they do not decrease, except at the very end of the tests, due to macroscopic cracking in the specimen. However, the variation of X shows a gradual

decrease: during the first cycles, X is about 70 MPa higher that R, whereas their respective values are equal at the end of the test. Thus, similarly to the case of Grade 91 steel [12], cyclic softening of Grade 92 steel during pure fatigue at 550°C is mainly due to a decrease in kinematic hardening i.e. to a decrease in long-range interactions, probably induced by the vanishing of low-angle subgrain boundaries often reported in the literature [14,15]. Concerning test 11, the significant noise which affects experimental data did not permit us to apply the Fournier's method to extract R, X and Σ_v. However, the hysteresis loops presented in Fig. 2 show similar trends for the two tests: a decrease in the value of X is also expected for test 11. Microstructural observations have been carried out in order to confirm these results.

3. Microstructural evolution

The microstructure of tempered martensite steels is composed of prior austenite grains, packets, blocks, laths and subgrains [16]. Evolution of this complex microstructure during fatigue, creep and creep-fatigue tests [3,14,17-19] is expected to affect softening. As precipitation is expected to be hardly affected by (short-term) pure fatigue at 550°C, the following microstructural observations focus on the evolution of subgrain size and dislocation density. Some of the typical effects resulting from long-term tests at high temperature (growth of $M_{23}C_6$ precipitates, formation of Laves phases and Z phase…) [19-21] are thus neglected in this study.

3.1. Experimental procedures

Subgrains were observed with a PHILIPS EM430 Transmission Electron Microscope (TEM) operated at 300 kV. Thin foils were taken from the as-received material and from the gauge length of specimens after tests 3 and 11, far from the fracture area and in a zone perpendicular to the loading axis. Small slices were cut and mechanically polished down to a thickness of 200 µm. For each of them, 3 mm diameter discs were punched and electrolytically thinned with a solution composed of 90 % ethanol and 10 % perchloric acid.

The size distribution of subgrains was determined from one typical TEM bright field picture for each sample with a magnification of 5500. Subgrains were manually traced on a transparent medium, followed by image processing with Matlab software. About 1,100 subgrains for the as-received material and about 400 subgrains for tests 3 and 11 samples were quantified on an area of interest of about 265 μm^2 for each material.

The average free dislocation density was determined from two TEM images of each sample with a mean linear intercept method using four randomly oriented segments per image [22]. The value of the average density was determined using Eq. 1 with e the local thickness of the thin foil (assumed to be about 0.15 µm), n_i the number of intersections between a segment and a dislocation and l_i the length of a segment:

$$\rho = \frac{2\sum_i n_i}{e\sum_i l_i} \qquad (1)$$

3.2. Evolution of hardness and damage development

The as-received Grade 92 steel shows a macrohardness of 224 ± 4 HV_{30} in sections both parallel and perpendicular to the pipe axis. Fatigue specimens show a slight decrease in hardness i.e. 210 ± 4 HV_{30} after test 3 and 207 ± 4 HV_{30} after test 11 far from the fractured surface. No significant effect of strain rate was evidenced.

Study of damage was rigorously carried out for Grade 91 by Fournier et al. [23] and permitted to exclude the influence of this phenomenon on the sensitivity of this kind of material to softening. Moreover, even if the cumulated viscoplastic deformation is high during PF tests, a previous study showed that cavitation has no influence on softening for Grade 92 during tensile tests [9]. As growth of cavities during uniaxial deformation was not significant in the uniformly strained part of the gauge length, even for low strain rates, it seems that softening is mainly due to microstructural evolution.

3.3. Evolution of dislocation structure

Microstructural evolution of tempered martensite during high temperature mechanical loading is well known [18-21]. Short-term PF tests on Grade 91 steel induced a modification of subgrain size distribution and a decrease in average free dislocation density [7-8]. TEM observations of the present study clearly show that numerous laths and subgrains of the as-received microstructure coarsened during PF tests (Fig. 5). A wider size distribution of subgrains is observed after PF tests (average sizes equal to 0.70 ± 0.05 µm and 0.74 ± 0.05 µm for tests 3 and 11 respectively) than in the as-received material (average size equal to 0.43 ± 0.05 µm), due to a heterogeneous increase in size of subgrains (Fig. 6). Fig. 6(b) shows that a lower strain rate induces a slightly wider distribution of subgrain size. This slight difference may have an influence on the slightly higher softening rate during test 11 with respect to test 3.

Regarding the decrease in average free dislocation density during PF tests, TEM observations (Fig. 5) show a lower free dislocation density after PF (~ 10^{14} m^{-2} for test 3), especially for the lowest strain rate (~ 3 10^{13} m^{-2} for test 11) compared to the as-received material (~ 2 10^{14} m^{-2}), in agreement with the observed cyclic softening.

The microstructural mechanisms responsible for softening are based on the disappearance of subgrain boundaries, composed of dislocation networks, induced by their annihilation with mobile dislocations that glide during viscoplastic deformation (see detailed description in [9,15]). In the present study, a simple homogenization model was introduced, using the mechanical effects of the evolution of the dislocation network induced by low cycle fatigue in order to predict the macroscopic behavior of Grade 92 steel.

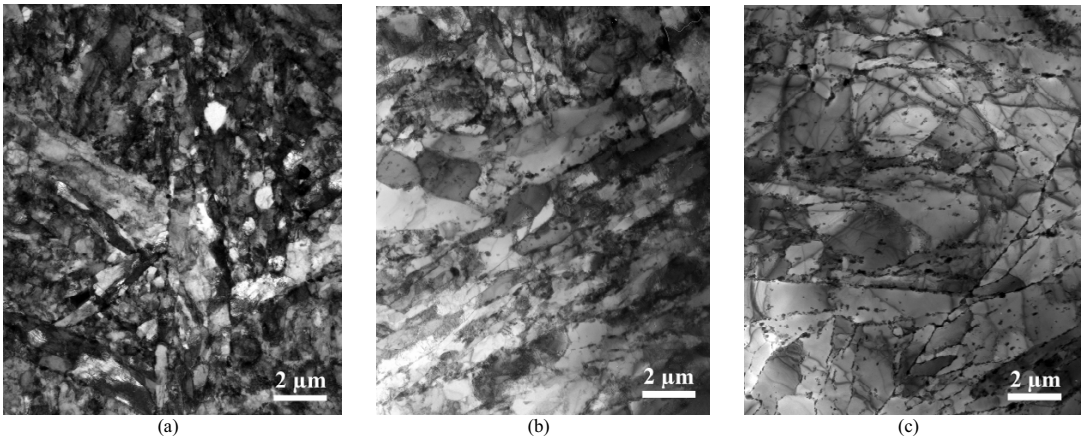

Fig. 5. TEM observations of the microstructure (a) in the as-received material, (b) after test 3 and (c) after test 11

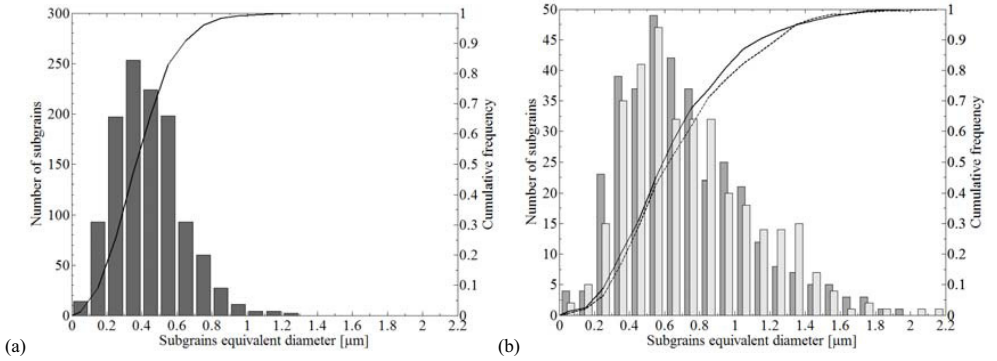

Fig. 6. Subgrain size distribution and corresponding cumulative frequency (a) for as-received material (average 0.43 ± 0.05 µm) and (b) after test 3 (average 0.70 ± 0.05 µm, dark grey and black continuous line) and after test 11 (average 0.74 ± 0.05 µm, bright grey and black dotted line)

4. Modeling cyclic behavior and metallurgical evolution during fatigue

4.1. Description of the model

The model presented in this paper is a simple mean field model based on polycrystalline elastoplasticity. Equations described in this part were implemented in SiDoLo software. Simulations were carried out considering a body-centered cubic (BCC) polycrystal composed of 50 crystals (here, martensite blocks) with randomly distributed crystal orientations. BCC crystal structure requires considering two families of slip systems – {110} and {112} planes and <111> slip directions – which altogether mean 24 slip systems.

In a first approximation, the model is based on Kröner's model [11] and the localization rule is given by the interaction law as follows:

$$\boldsymbol{\sigma} = \boldsymbol{\Sigma} + 2\mu(1-\beta)\left(\mathbf{E}^{\mathrm{P}} - \boldsymbol{\varepsilon}^{\mathrm{P}}\right) \tag{2}$$

In Eq. 2, β is a constant equal to $2(4 - 5\nu)/15(1 - \nu)$ [11]; μ is the shear modulus equal to 68 GPa; ν is the Poisson's ratio equal to 0.3; $\boldsymbol{\sigma}$ and $\boldsymbol{\Sigma}$ are respectively the local (i.e. in the considered block) and macroscopic stress tensors and $\boldsymbol{\varepsilon}^{\mathrm{P}}$ and $\mathbf{E}^{\mathrm{P}}$ are respectively the local and macroscopic plastic strain tensors. Considering one block and one slip system i, the shear stress τ^i is expressed in Eq. 3, resulting from the projection of the local stress tensor $\boldsymbol{\sigma}$ on i^{th} slip system.

$$\tau^i = \boldsymbol{\sigma} : \left(\mathbf{m}^i \otimes \mathbf{n}^i\right) \tag{3}$$

In Eq. 3, $\mathbf{m}^i$ is the slip direction and $\mathbf{n}^i$ is the normal to the slip plane. The critical shear stress τ_{c} corresponding to the sum of the critical shear stress on each of the 24 slip systems and required to activate the plastic slip, is supposed to be the same for all slip systems. It is expressed as:

$$\tau_{\mathrm{c}} = \tau_0 + \alpha\mu b\sqrt{\rho_{\mathrm{e}} + \rho_{\mathrm{s}}} \tag{4}$$

In Eq. 4, α is a constant equal to 0.35 for BCC crystals [24]. As the Peierls stress is close to zero for temperature higher than 400 K [25], τ_0 is taken equal to zero. Other obstacles, such as MX precipitates, are not taken into account in this simple model; the influence of this hypothesis is discussed later. The Burgers vector magnitude b is equal to 0.254 nm. In this model, the distinction between edge and screw dislocations (with respective total free dislocation densities ρ_{e} and ρ_{s}) is required as explained later. Both average free dislocations densities ρ_{e} and ρ_{s} are considered as homogeneously distributed in the matrix: thus, each of the 24 slip systems i is characterized by two free dislocation densities $\rho_{\mathrm{e}}{}^i$ and $\rho_{\mathrm{s}}{}^i$ respectively equal to $\rho_{\mathrm{e}}/24$ and $\rho_{\mathrm{s}}/24$ in the as-received condition. Here, subgrain boundaries are considered as networks of edge or screw dislocations [26]. Following this hypothesis, viscoplastic slip and evolution of dislocation density are expressed separately for edge and screw dislocations. Viscoplastic slip on slip system i requires a positive effective stress A^i, defined as:

$$A^i = \left|\tau^i - x^i\right| - \tau_{\mathrm{c}} \tag{5}$$

x^i is the local kinetic hardening (its evolution is described in Eq. 10). Following the theory of thermally activated processes [27], if A^i is positive, the viscoplastic slip rates are expressed for edge and screw dislocations respectively by:

$$\dot{\gamma}_e^i = \nu_0 b^2 \rho_e^i \exp\left(-\frac{Q}{kT}\right)\sinh\left(\frac{V A^i}{kT}\right) \text{ and } \dot{\gamma}_s^i = \nu_0 b^2 \left(\sum_{j\in\Omega}\rho_s^j\right)\exp\left(-\frac{Q}{kT}\right)\sinh\left(\frac{V A^i}{kT}\right) \tag{6}$$

In Eq. 6, ν_0 is a vibration frequency relative to jump over an obstacle and is equal to about 10^{13} s^{-1}. Parameters k, T, Q and V are respectively the Boltzmann constant, the testing temperature, the activation energy and the activation volume. Ω is the set of slip systems containing screw dislocations having the same Burgers vector as the considered screw dislocation. For a given slip system i and a given dislocation type (edge or screw), the evolution of average misorientation is expressed as:

$$\dot{\theta}_e^i = -\theta_e^i \frac{y_e}{b}\left|\dot{\gamma}_e^i\right| \text{ and } \dot{\theta}_s^i = -\frac{y_s}{b}\sum_{j\in\Omega}\left(\theta_s^j\left|\dot{\gamma}_s^j\right|\right) \quad (7)$$

y_e (resp. y_s) is the athermal edge (resp. screw) annihilation distance, equal to about 6b (resp. 200b) for copper at room temperature [28]. Subgrain boundaries are here considered to be composed of either edge or screw dislocation types in equal quantities. Their corresponding misorientations (θ_e^i and θ_s^i respectively) are weighted values of the misorientation of each subgrain boundary type. The diameter d of subgrains is calculated simply using Eq. 8, θ and d_{block} being the average subgrain misorientation and the average size of blocks, respectively.

$$d = \frac{d_0 - d_{block}}{\theta_0}\theta + d_{block} \text{ with } \theta = \sum_{i=1}^{24}\left(\theta_e^i + \theta_s^i\right) \quad (8)$$

In Eq. 8, d_0 is the initial diameter of subgrains, equal to 0.43 µm (see previous section) and θ_0 is the initial average misorientation equal to 1.7° [29]. As total free dislocations densities, θ_0 is considered as homogeneously distributed in the matrix: in as-received condition, both θ_e^i and θ_s^i are equal to $\theta_0/48$. Based on a Hall-Petch-like formulation, the maximal kinematic stress for one given slip system was expressed by Li [30] as follows, with θ_{block} the misorientation between two blocks:

$$x_{\max}^i = \frac{\mu}{1-\nu}\sqrt{\frac{0.45b}{2\pi}}\left\{\left[1-\left(\frac{d}{d_{block}}\right)^3\right]\sqrt{\frac{\theta}{d}} + \left(\frac{d}{d_{block}}\right)^3\sqrt{\frac{\theta_{block}}{d}}\right\} \quad (9)$$

θ_{block} and d_{block} were taken from EBSD measurements on a Grade 91 steel [31]. During one cycle, the evolution of the local kinematic hardening on each slip system is described by:

$$\dot{x}^i = C\left[sign\left(\tau^i - x^i\right) - \frac{x^i}{x_{\max}^i}\right]\left|\dot{\gamma}_e^i + \dot{\gamma}_s^i\right| \quad (10)$$

The function $sign(\tau^i - x^i)$ is set to +1 if $(\tau^i - x^i)$ is positive and -1 if $(\tau^i - x^i)$ is negative. In the present paper, the dislocation density during cycling is considered as constant: at present, neither softening nor evolution of isotropic hardening is taken into account (in fact, isotropic hardening has been shown in previous sections to be constant). Consequently, the identification of model parameters was performed on the first cycle of test 3.

4.2. Identification of model parameters

The set of parameters and their values required for the model are presented in Table 3. Only three of them (Q, V and C) were adjusted for predicting the hysteresis loop of test 3 as accurately as possible.

Table 3. Parameters and their value required for the model. Fixed parameters were estimated from literature or from simplifying assumptions and adjusted parameters were optimized by an iterative method

Universal constants and microstructural parameters evaluated from the as-received condition and observations of first loop of test 3								
ν	0.3		T	823 K		θ_{block}	30 °	[31]
μ	68 GPa		y_e	2 nm	[28]	d_0	0.43 µm	
ν_0	10^{13} s^{-1}	[27]	y_s	50 nm	[28]	d_{block}	2.3 µm	[31]
b	2.54 10^{-10} m		$\rho = \rho_e + \rho_s$	2 10^{14} m^{-2}				
k	1.38 10^{-23} J.K^{-1}		θ_0	1.7 °	[29]			
Fixed parameters						Optimized parameters		
α	0.35	[24]				Q	1.3 eV	
τ_0	0 MPa	[25]				V	110 b^3	
						C	406,800 MPa	

The results of the model are presented for the first cycle in Fig. 7.

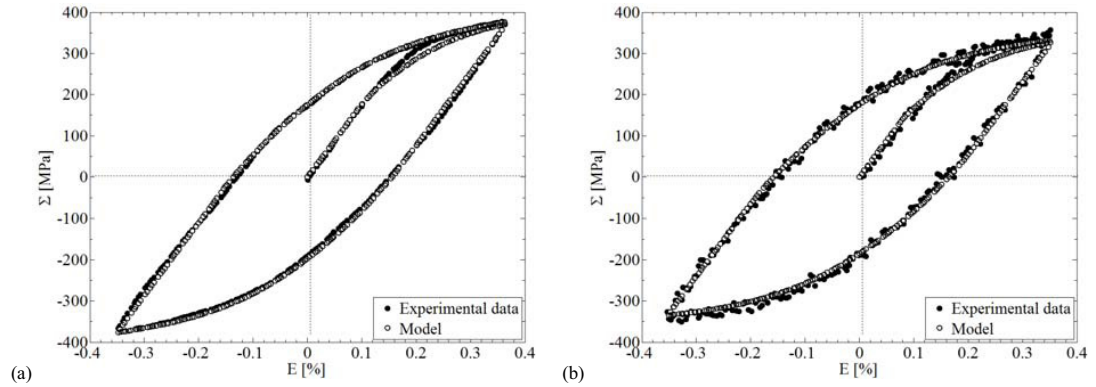

Fig.7. First hysteresis loop recorded and the corresponding model prediction using parameters from Table 3 (a) for test 3 and (b) for test 11

Although only three parameters were adjusted, the model shows good agreement with experimental stress-strain curves and with the expected strain rate sensitivity. The difference between experimental data and predicted curve on the first tensile load is due to the simplified hypothesis of neglecting the strengthening effect induced by precipitates in the tempered martensite matrix. Considering the values of adjusted parameters, the activation volume V is similar to the value corresponding to fatigue-induced plastic deformation (about 100 b^3) and the activation energy Q is lower than that of typical diffusion processes in ferrite (about 2.5 eV). These results are nevertheless in agreement with literature: the corresponding values are significantly scattered because they strongly depend on the material, experimental conditions and technique that are used [12]. The small value of V suggests that viscoplastic deformation is driven by phenomena taking place at a scale finer than the subgrain size.

The macroscopic strain rate sensitivity is well predicted by the model. However, cyclic softening is not taken into account in this present study yet: the first improvement of the model will be to implement the evolution of free dislocation density during fatigue testing. Other main improvements will concern the localization law used in the model and the maximal kinematic stress evolution. A localization law adapted from the approach of Molinari et al. [32] will be implemented in the model in order to better approximate the elastic-viscoplastic behavior of these steels: indeed, the present Kröner's localization rule does not permit us to predict accurately loading involving significant viscoplastic deformation, such as relaxation or creep. Eq. 9 formulated by Li will be replaced by another model in better accordance with experimental observations. Finally, misorientations between subgrains that are more realistic with respect to the tempered martensite microstructure will be considered.

5. Conclusions

Pure fatigue tests at two different strain rates ($2\ 10^{-3}\ s^{-1}$ and $10^{-5}\ s^{-1}$) were carried out at 823 K on Grade 92 steel. Experimental results and model prediction lead to the following conclusions:

1. Cyclic softening depends on the strain rate: the lower the strain rate, the more pronounced the cyclic softening.
2. Cyclic softening is mainly due to a decrease in the kinematic part of hardening during the fatigue test. TEM observations show that this is induced by an increase in subgrain size and a decrease in free dislocation density. These evolutions are more pronounced for the lower strain rate.
3. The model gives a good prediction of the influence of strain rate on the macroscopic mechanical behavior during the first cycles. However, it has to be improved to describe softening due the evolution of subgrain size and free dislocation density during further cycling.

Acknowledgments

The authors express their thanks to Vallourec & Mannesmann Tubes for providing the material, and are grateful to E. Cini from Vallourec for fruitful discussions.

References

[1] Greeff AP, Louw CW, Swart HC. The oxydation of industrial FeCrMo steel. *Corros Sci* 2000;**42**:1725-1740

[2] Toloczko MB, Hamilton ML, Maloy SA. High temperature tensile testing of modified 9Cr-1Mo after irradiation with high energy protons. *J Nucl Mater* 2003;**318**:200-206

[3] Shankar V, Valsan M, Bhanu Sankara Rao K, Kannan R, Mannan SL, Pathak SD. Low cycle fatigue behavior and microstructural evolution of modified 9Cr-1Mo ferritic steel. *Mater Sci Eng A* 2006;**437**:413-422

[4] Sklenička V, Kuchařová K, Svoboda M, Kloc L, Buršík J, Kroupa A. Long-term creep behavior of 9-12%Cr power plant steels. *Mater Charact* 2003;**51**:35-48

[5] Armas AF, Petersen C, Schmitt R, Avalos M, Alvarez-Armas I. Mechanical and microstructural behaviour of isothermally and thermally fatigued ferritic/martensitic steels. *J Nucl Mater* 2002;**307-311**:509-513

[6] Polcik P, Sailer T, Blum W, Straub S, Buršík J, Orlová A. On the microstructural development of the tempered martensitic Cr-steel P91 during long-term creep – a comparison of data. *Mater Sci Eng A* 1999;**260**:252-259

[7] Pešička J, Kužel R, Dronhofer A, Eggeler G. The evolution of dislocation density during heat treatment and creep of tempered martensite ferritic steels. *Acta Mater* 2003;**51**:4847-4862

[8] Dubey JS, Chilukuru H, Chakravartty JK, Schwienheer M, Scholz A, Blum W. Effects of cyclic deformation on subgrain evolution and creep in 9-12% Cr-steels. *Mater Sci Eng A* 2005;**406**:152-159

[9] Giroux PF, Dalle F, Sauzay M, Malaplate J, Fournier B, Gourgues-Lorenzon AF. Mechanical and microstructural stability of P92 steel under uniaxial tension at high temperature. *Mater Sci Eng A*, in press (2010)

[10] Cottrell AH. *Dislocations and plastic flow in crystals*. Oxford University Press; 1953

[11] Kröner E. Zur plastischen Verformung des Vielkristalls. *Acta Metall* 1961;**9**:155-161

[12] Fournier B, Sauzay M, Caës C, Noblecourt M, Mottot M. Analysis of the hysteresis loops of a martensitic steel. Part I. *Mater Sci Eng* 2006;**437**:183-196

[13] Lemaitre J, Chaboche JL. *Mechanics of solids materials*. Springer-Verlag; 1987

[14] Eggeler G, Nilsvang N, Ilschner B. Microstructural changes in a 12% chromium steel during creep. *Steel Res* 1987;**58-2**:97-103

[15] Sauzay M. Modelling of the evolution of micro-grain misorientations during creep of tempered martensite ferritic steels. *Mater Sci Eng* 2009;**510-511**:74-80

[16] Marder JM, Marder AR. The morphology of iron-nickel massive martensite. *Trans ASM* 1969;**62**:1-10

[17] Orlová A, Buršík J, Kuchařová K, Sklenička V. Microstructural development during high temperature creep of 9%Cr steel. *Mater Sci Eng A* 1998;**245**:39-48

[18] Abe F. Evolution of microstructure and acceleration of creep rate in tempered martensitic 9Cr-W steels. *Mater Sci Eng A* 1997;**234-236**:1045-1048

[19] Ennis PJ, Zielinska-Lipiec A, Wachter O, Czyrska-Filemonowicz A. Microstructural stability and creep rupture strength of the martensitic steel P92 for advanced power plant. *Acta Metall* 1997;**45-12**:4901-4907

[20] Eggeler G. The effect of long-term creep on particle coarsening in tempered martensite ferritic steels. *Acta Metall* 1989;**37-12**:3225-3234

[21] Hald J. Microstructure and long-term creep properties of 9-12% Cr steels. *Int J Pres Ves & Piping* 2008;**85**:30-37

[22] Klaar H, Schwaab P, Österle W. Round robin investigation into the quantitative measurement of dislocation density in the electron microscope. Prakt Metallogr 1992;**29**:3-25

[23] Fournier B, Sauzay M, Caës C, Noblecourt M, Mottot M, Bougault A, Rabeau V, Pineau A. Creep-fatigue-oxidation interactions in a 9Cr-1Mo martensitic steel. Part I: Effect of tensile holding period on fatigue lifetime. *Int J Fatigue* 2008;**30**:649-662

[24] Devincre B, Kubin L, Hoc T. Physical analyses of crystal plasticity by DD simulations. *Scr Mater* 2006;**54**:741-746

[25] Sommer C, Mughrabi H, Lochner D. Influence of temperature and carbon content on the cyclic deformation and fatigue behaviour of α-iron. Part I. Cyclic deformation and stress-behaviour. *Acta Mater* 1998;**46-5**:1527-1536

[26] Read WT, Shockley W. Dislocation models of crystal grain boundaries. Phys Rev 1950;78-3:275-289

[27] Caillard D, Martin JL. *Thermally activated mechanisms in crystal plasticity*. Vol 8. Pergamon Materials Series; 2003

[28] Essmann U, Mughrabi H. Annihilation of dislocations during tensile and cyclic deformation and limits of dislocation densities. *Philos Mag* 1979;**40**:731-756

[29] Tak KG, Schulz U, Eggeler G. On the effect of micrograin crystallography on creep of FeCr alloys. *Mater Sci Eng A* 2009;**510-511**:121-129

[30] Li JCM. Petch relation and grain boundary sources.*Trans Metall Soc AIME* 1963;**227**:239-247

[31] Fournier B. *Fatigue-fluage des aciers martensitiques à 9-12%Cr : comportement et endommagement*. PhD Thesis. Ecole des Mines de Paris; 2003

[32] Molinari A, Ahzi S, Kouddane R. On the self-consistent modeling of elastic-plastic behavior of polycristal. *Mech Mater* 1997;**26**:43-62